Supporting Material

Bacterial Motility Reveals Unknown Molecular Organization

Ismaël Duchesne, Simon Rainville and Tigran Galstian*

*Department of Physics, Engineering Physics and Optics and Center for Optics, Photonics and Lasers, Laval University, Quebec City, Canada G1V 0A6

S1 Linear correlation between the mean squared displacement (MSD) and the time

The diffusion of particles in a liquid crystal (LC) can be in normal or anomalous regimes depending upon the time scale used to record their movements [1, 2]. The anomalous behavior is characterized by a non-linear relation between the mean squared displacement (MSD) and time, whereas the normal diffusion corresponds to a linear relationship. By plotting the MSD for our viscosity measurements as a function of time, we obtained a linear relation at every concentration, which indicates normal diffusion [3]. To quantify this linear relationship, we computed the linear correlation coefficient (also known as the Pearson product-moment coefficient of correlation) of the relation between the MSD and the time for a short period of time (10 first frames) and for a longer period (50 first frames). As we can see in Fig. S1, the coefficient is always very close to 1, which mean a very good linear relation. This result is in agreement with [3] where normal diffusion was also obtained for the same time scale (minimum sample rate of 0.4 s) but with DSCG solution in deionized water.

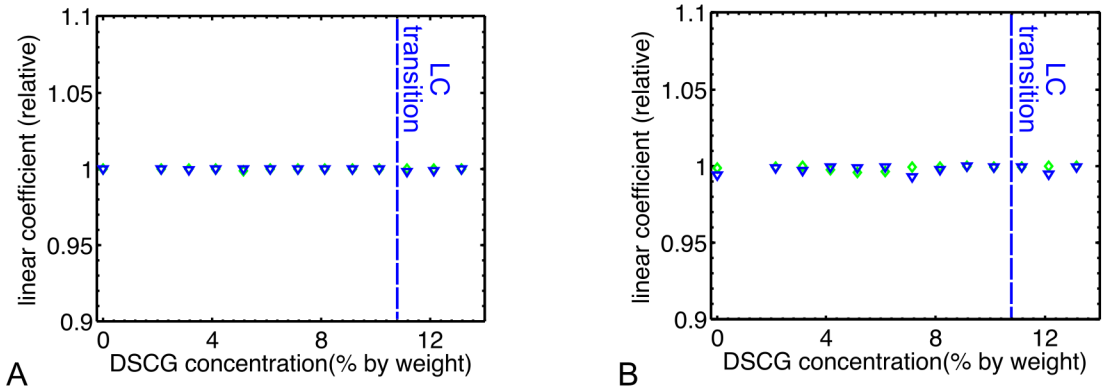

Figure S1: Linear coefficient of the mean squared displacement vs time showing that the diffusion is normal (at every DSCG concentration). (A) Linear coefficient computed from the first 10 data points and (B) from the first 50 data points. The green diamonds were calculated from the viscosity parallel to $\mathbf{n}$ and the blue triangles from the viscosity perpendicular to $\mathbf{n}$. At each concentration, the probability to obtain the same coefficient value with a random distribution was estimated to be $\leq 10^{-16}$.

S2 Propulsive force and variable torque regime

The flagellar motor of the bacteria can work in two regimes [4]. The first one appears when the motor rotates at low angular speed, below the critical angular speed ω_m^c (see Fig. S2*A*). In this regime, the torque of the motor remains constant when its angular speed changes. Thus, the torque applied by the motor is not modified when the load (here, the viscosity of the medium) changes. In the second regime, when the motor rotates at an angular speed higher than ω_m^c, the torque decreases linearly with increasing angular speed until it becomes 0 when the maximum angular speed (ω_m^{max}) is reached. Consequently, the torque produced by the motor increases when the load (or viscosity) is raised. This section will show that the torque increase cannot explain the increase in the propulsive force in the pretransition zone and in the anisotropic phase, even if both the constant and variable regimes seem to be present in our experiments.

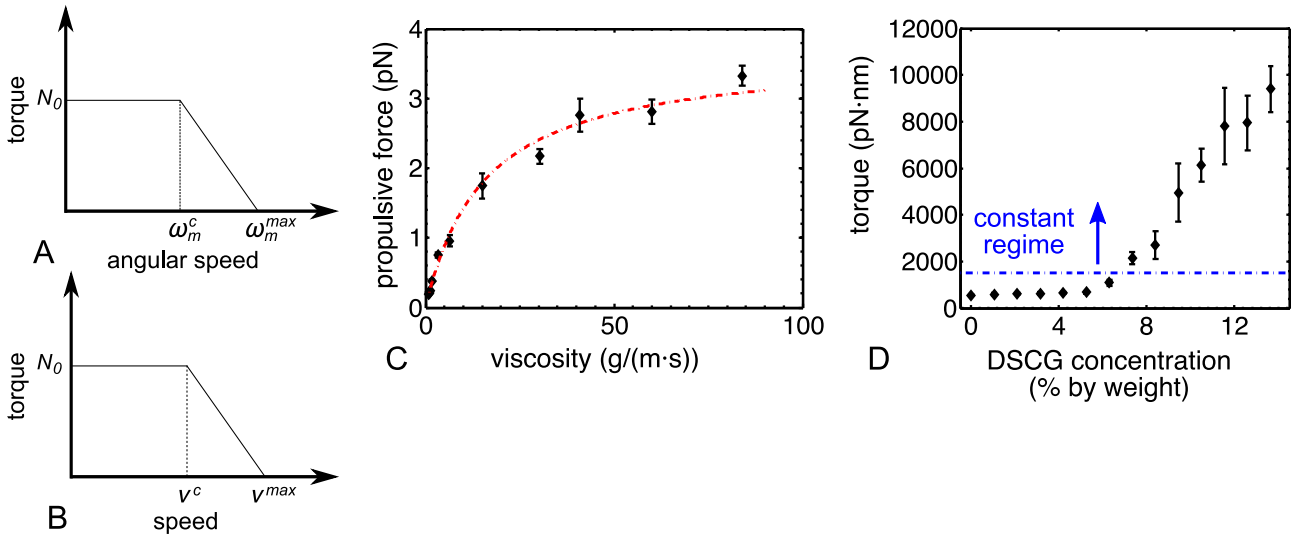

Figure S2: Relationship between the torque (exerted by the motor), the angular speed of the motor and the speed of the bacteria. (*A*) Schematic of the torque produced by the motor on its angular speed and (*B*) on the speed of the bacteria. (*C*) Estimation of the propulsive force produced by the bacteria as a function of the viscosity of the DSCG solutions. (*D*) Equivalent stall torque (N_0) as a function of the DSCG concentration computed with the propulsive force in *C* by considering a constant torque regime. The dotted line in *C* represents the best fit of the propulsive force computed by using the Purcell's model in the variable torque regime (Eq. S12). The average known stall torque N_0 for *E. coli* is shown with the dotted line in *D* [4,5].

The Purcell's model describes the forces involved when a bacterium swims in a Newtonian liquid. In this model, the bacterium is described by a prolate spheroid and it has only one filament at one of its poles. The forces and the torques on the body and the filament are described by [5,6]

$$F_b = -A_0 v, \tag{S1}$$

$$N_b = -D_0 \Omega, \tag{S2}$$

$$F_f = -Av - B\omega \tag{S3}$$

and

$$N_f = -Bv - D\omega, \tag{S4}$$

where v is the speed of the bacterium, Ω is the angular speed of the body, ω is the angular speed of the filament (negative), and A_0, D_0, A, B and D depend linearly on the viscosity. Since the total force and

torque must be zero for a stationary movement of bacterium (no external forces applied), we can solve these equations to obtain the relation between the speed, ω and Ω [5]:

$$v = \frac{B}{A_0 + A}\omega \equiv \gamma\omega, \tag{S5}$$

$$v = \frac{D(A_0 + A) - B^2}{D_0 B}\Omega \equiv R_1\Omega, \tag{S6}$$

where γ and R_1 are independent of the viscosity. The angular speed of the motor is given by the addition of the rotations of the body and the filament. With the equations above we obtain a relation between the angular speed of the motor and the speed of the bacterium:

$$\omega_m = \omega + \Omega = (\gamma^{-1} + R_1^{-1})v. \tag{S7}$$

We can see that the speed of the bacterium and the angular speed of the motor are two equivalent quantities that are proportional to each other. Thus, the relationship between the torque and the speed of the bacterium comprises the same two regimes mentioned above for the angular speed of the motor (see Fig. S2B). From Eq. S6 above and Eqs. 10a and 10b from [5] we obtain the dependence of the speed on the viscosity for the two regimes of torque (constant or variable):

$$\text{if } \omega_m < \omega_m^c\,, \quad v = \frac{N_0}{D_0 R_1} \equiv \frac{N_0}{d_0 R_1 \eta}, \tag{S8}$$

$$\text{if } \omega_m > \omega_m^c\,, \quad v = \frac{\alpha_v v^{max}}{D_0 R_1 + \alpha_v} \equiv \frac{\alpha_v v^{max}}{d_0 R_1 \eta + \alpha_v}, \tag{S9}$$

where

$$\alpha_v = \left|\frac{dN}{dv}\right| = \frac{N_0}{v^{max} - v^c}, \tag{S10}$$

$D_0 = \frac{16\pi\eta ab^2}{3}$ with a and b being the semi-major and semi-minor axes of the prolate spheroid, N_0 is the stall torque and $d_0\eta = D_0$. In the two regimes, the drag force (used as the approximation of the propulsive force) on the body of the bacteria (Eq. S1) becomes

$$\omega_m < \omega_m^c: \quad F_b = A_0\frac{N_0}{D_0 R_1} \equiv \frac{a_0 N_0}{d_0 R_1}, \tag{S11}$$

$$\omega_m > \omega_m^c: \quad F_b = A_0\frac{\alpha_v v^{max}}{D_0 R_1 + \alpha_v} \equiv \frac{a_0\alpha_v v^{max}}{d_0 R_1 + \alpha_v \eta^{-1}}, \tag{S12}$$

where $a_0\eta = A_0$. As we can see, the propulsive force does not depend on the viscosity in the low speed regime, but it does in the high speed regime. The values of the constants in the above equations are:

$$A = k_n L \sin\Psi \tan\Psi(1 + \gamma\cot^2\Psi)\eta, \tag{S13}$$

$$B = k_n L\frac{\lambda}{2\pi}\sin\Psi\tan\Psi(1 - \gamma)\eta, \tag{S14}$$

$$D = k_n L\left(\frac{\lambda}{2\pi}\right)^2\sin\Psi\tan\Psi(1 + \gamma\cot^2\Psi)\eta, \tag{S15}$$

$$A_0 = \frac{4\pi a}{\ln\frac{2a}{b} - \frac{1}{2}}\eta, \tag{S16}$$

$$D_0 = \frac{16\pi}{3}ab^2\eta, \tag{S17}$$

with

$$k_n = \frac{8\pi}{2\ln\frac{c\lambda}{r} + 1}, \tag{S18}$$

$$k_t = \frac{4\pi}{2\ln\frac{c\lambda}{r} - 1}, \tag{S19}$$

where $L = 7\,\mu$m is the length of the filament, $\Psi = 41\,^\circ$ is the angle made by the flagellar filament with the flagellar axis, $\gamma = \frac{k_t}{k_n}$, $\lambda = 2\,\mu$m is the pitch of the filament, $r = 20\,$nm is the estimated radius of the tube that composed the filament and $c = 2.4$ is the Lighthill constant [5, 7].

As we can see in Fig. S2*C* the propulsive force increases when the viscosity of the DSCG solution is raised. To find out whether this increase in the propulsive force is caused by the increase of the torque exerted by the motor, we draw the equivalent stall torque N_0 for each DSCG concentration using the constant torque regime equation (Eq. S11). The value of N_0 varies from $550 \pm 26\,\mathrm{pN \cdot nm}$ to $9400 \pm 980\,\mathrm{pN \cdot nm}$ (see Fig. S2*D*). From [4,5], N_0 should be around $1500\,\mathrm{pN \cdot nm}$ for *E. coli*, so the constant regime should be reached between 6.2 wt% and 7.2 wt% (see the blue line in Fig. S2*D*). Therefore the torque of the bacteria should be variable only for the concentrations below 7.2 wt% and the propulsive force should be constant at concentrations above. Furthermore, the increase in the torque of the bacteria cannot explain why N_0 reaches $9000\,\mathrm{pN \cdot nm}$ at high DSCG concentration, a value far away from the known N_0 for *E. coli* (around $1500\,\mathrm{pN \cdot nm}$).

To complete our analysis, we fitted the dependence of the propulsive force on the viscosity with Eq. S12 (dotted line in Fig. S2*C*) by using $N_0 = 1500\,\mathrm{pN \cdot nm}$. The model correlates very well with our data when $v^c = 13.6 \pm 0.4\,\mu$m/s and $v^{max} = 15.9 \pm 0.5\,\mu$m/s. Here again, the torque should be variable only above a speed of $v^c = 13.6 \pm 0.4\,\mu$m/s, which correspond to a DSCG concentration below 8.2 wt% (see Fig. 2*A* of the paper). By using Eq. S7, we computed the equivalent angular speed of the motor and obtained $\omega_m^c = 61 \pm 2\,$Hz and $\omega_m^{max} = 71 \pm 2\,$Hz. These values are far away from known values with $\omega_m^c \sim 150\,$Hz and $\omega_m^{max} \sim 300\,$Hz [4]. Consequently, the variable torque cannot explain the increase in the propulsive force observed in the pretransition zone and anisotropic phase.

In summary, the variable torque regime could explain the increase in the propulsive force only below a DSCG concentration of 7.2 wt%, namely at the beginning of the pretransition zone and before. The additional increase of the propulsive force must be caused by another phenomenon. We think that, in the pretransition zone and anisotropic phase, the solution becomes highly non-Newtonian and this is why the Purcell's model cannot explain the increase of the propulsive force. The presence of the non-Newtonian medium would increase the propulsive force by increasing its efficiency (see paper for more information).

S3 Estimation of the depletion force in the pretransition zone

In a solution of large particles with much smaller rods with a diameter D and a length L, the depletion effect can cause the aggregation of the large particles. At first order in rods concentration, in the particular case where the particles are spheres of radius R and $D \ll L \ll R$, the depletion energy between two spheres is described by [8, 9]

$$U(h) = \frac{\pi k_B T n_r R L^2}{6} \left(\frac{h}{L} - 1 \right)^3, \tag{S20}$$

where k_B is the Boltzmann constant, T the temperature in Kelvin, n_r the number density of the rods and h is the distance between the surface of the spheres. This equation holds only for $0 \leq h \leq L$ since there is no depletion effect when the distance between the spheres is larger than L. Experimentally, we observed that bacteria are sometimes able to detach themselves from aggregates of bacteria or surfaces in the pretransition zone. We thus suppose that the phenomenon responsible for the sticky effect can apply a force similar to the propulsive force. To compare the strength of the depletion effect and of the propulsive force of the bacteria, the depletion force was derived from Eq. S20 :

$$F_d(h) = \frac{dU(h)}{dh} = \frac{\pi k_B T n_r R L}{2} \left(\frac{h}{L} - 1 \right)^2. \tag{S21}$$

Table S1: Measured and computed volume concentration and characteristics of DSCG solutions.

Concentration (± 0.2) (wt %)	Measured concentration (vol %)	Computed concentration (vol %)	Number density (10^{24} rods/m^3)	Aggregates length (nm)
0	0	0	—	—
2.2	1.4 ± 0.2	1.36	—	—
3.2	2.0 ± 0.3	2.00	—	—
4.2	2.7 ± 0.3	2.64	—	—
5.2	3.3 ± 0.3	3.29	—	—
6.2	3.9 ± 0.3	3.94	3.9 ± 0.5	6 ± 1
7.2	4.6 ± 0.4	4.60	2.7 ± 0.3	11.0 ± 0.4
8.2	5.2 ± 0.4	5.27	2.7 ± 0.3	12.4 ± 0.7
9.2	5.8 ± 0.5	5.93	2.8 ± 0.3	13.4 ± 0.7
10.2	6.5 ± 0.5	6.61	3.1 ± 0.3	13.5 ± 0.7
11.2	7.1 ± 0.5	7.29	3.7 ± 0.3	12.8 ± 0.7
12.2	7.7 ± 0.6	7.97	4.2 ± 0.4	12.2 ± 0.7
13.2	8.4 ± 0.6	8.66	4.8 ± 0.4	11.5 ± 0.7

To compute this force, we used $T = 295.65\,\mathrm{K}$ and the stokes radius of the bacteria as the radius of the sphere $R = 0.57 \pm 0.2\,\mu\mathrm{m}$ (see Eq. 8 of the paper). To obtain the number density of the rods we first measured the volume concentration of the DSCG molecules by comparing the motility buffer volume added to the solution to obtain the right weight concentration with the total volume of the final solution (see Table S1). The number density of the DSCG molecules was then computed with the following expression

$$n_{DSCG} = \frac{M_{DSCG} N_A}{M_w V_{tot}}, \tag{S22}$$

where M_{DSCG} is the mass of the DSCG in a given solution of total volume V_{tot}, N_A is the Avogadro constant and M_w is the molecular weight of the DSCG (512.33 g/mol). Finally to convert the number

density of molecules in terms of the number density of rods, we used the aggregation model presented in the paper. Indeed, each rod is made of a stack of disks with a thickness t_r of 0.34 nm and composed of two DSCG molecules. Thus, the equation below gives the number density of rods

$$n_r = \frac{n_{DSCG} t_r}{2L}. \tag{S23}$$

To verify whether our volume concentrations were consistent with the DSCG model described in the paper, we computed the theoretical volume fraction by using this model. For this purpose, the following expressions were used:

$$V_{H_2O} = \frac{M_{H_2O}}{\rho_{H_2O}}, \tag{S24}$$

$$V_{mol} = \frac{\pi r^2 L}{2}, \tag{S25}$$

$$N_{DSCG} = \frac{M_{DSCG} N_A}{M_w}, \tag{S26}$$

$$V_{DSCG} = N_{DSCG} V_{mol}, \tag{S27}$$

where M_{H_2O} is the mass of water in a solution, ρ_{H_2O} is the density of water, V_{mol} is the volume of one molecule of DSCG, r is the radius of the DSCG disk, N_{DSCG} is the number of DSCG molecules in the solution and V_{DSCG} is the volume occupied by the DSCG molecules in the solution. By comparing the theoretical results with our measurements (see Table S1) we can see that the difference between these two quantities is always $\leq 3.5\,\%$. Therefore, the model seem to be in good agreement with our measurements.

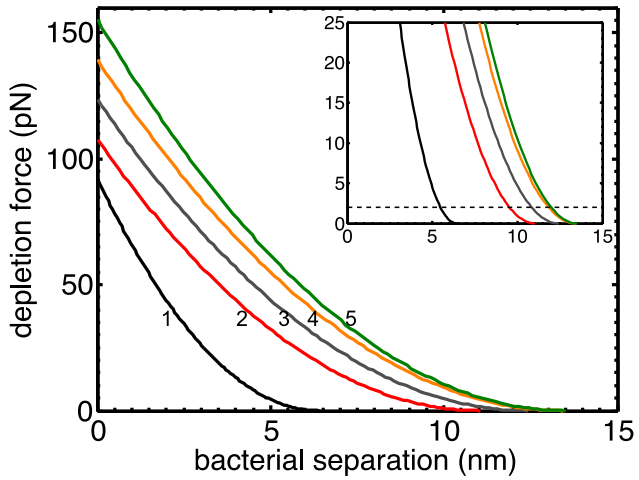

Figure S3: Estimated depletion force between two bacteria as a function of the distance between their surfaces. Each curve represents a different rod concentration: from left (1) to right (5), the concentration starts at 6.2 wt% and finishes at 10.2 wt% with an increment of 1 wt%. The dotted line in the inset shows the approximate value of the propulsive force in the pretransition zone (around 2 pN).

In Fig. S3 we can see the depletion force between two bacteria as a function of the distance between their surfaces for a DSCG concentration between 6.2 wt% and 10.2 wt%. By observing the maximal depletion force at each concentration, we observe that the strength of the depletion increases with concentration, which could explain why the bacteria become more and more sticky when the concentration is raised. Moreover, the depletion effect could be important in the sticky process of the bacteria since the maximum depletion force is always higher than the propulsive force of the bacteria in the pretransition zone (around 35 times higher at 6.2 wt% and 75 times higher at 10.2 wt%). This aspect could explain why the bacteria generally

remain stuck to surfaces or others bacteria in this zone. On the other hand, some bacteria are observed to detach themselves from aggregates of bacteria or others surfaces, and it is hard to believe that the propulsive force could reach a value as high as the maximum depletion force (even in the case where the propulsion of the two bacteria adds up). Indeed we can see in the inset of Fig. S3 the minimum distance between two bacteria where they are able to detach themselves using their propulsion only. This distance is around 5 nm at 6.2 wt% and 12 nm at 9.2 wt%. In is thus possible that the filament could momentarily create a perturbation in the depletion force, which could cause one bacterium to move a few nanometers away from the other, allowing it to detach. Furthermore, bacteria have many proteins that partially emerge from their membrane, and create some protuberance on their surface (on the nm scale). The surface of two bacteria (or one bacterium and the wall of the chamber) are probably never completely in contact, causing the depletion force to be smaller than the one computed.

We conclude that the depletion effect could explain the sticky behavior observed in the pretransition zone.

S4 Effect of reactive oxygen on the speed of the bacteria

When a fluorophore is exposed to light in the presence of atmospheric oxygen (O_2), it looses its fluorescence with time (photobleaching). This reaction creates reactive oxygen, for example singlet oxygen ($^1O_2$) and superoxide [10, 11]. These reactive forms will perturb the viability of the bacteria cell by breaking the proteins, DNA or lipid chains. To verify whether this effect can explain the discrepancy between our speed measurements and the speed obtained in [12], we recorded movies of swimming bacteria while they were exposed to light with and without fluorophore. To do so, a X-cite 120LED (Lumen dynamic, ON, Canada) with a blue filter at 482 nm (bandwidth of 35 nm) was used to illuminate the sample. The first experiments were made in motility buffer in presence of oxygen and the second, after the bacteria had consumed all the oxygen. As we can see on Fig. S4 *A* and *B*, the bacteria in both solutions do not seem to be sensitive to light. In contrast, when 0.01 mM of Syto 9 (from the Invitrogen Live Dead kit, the same fluorophore used in [12]) is added to the solution, the speed of the bacteria in an oxygenated solution decreases with increasing light intensity (see Fig. S4*C*). On the other hand, the bacteria in solution without oxygen remain unaffected by light (see Fig. S4*D*). Furthermore, in solutions with a higher concentration of bacteria, they seem to be less sensitive to the light. This could be caused by the fact that, at the moment of the experiments, the bacteria had consumed more oxygen, and also because the fluorophore concentration was higher in the concentrated bacteria solutions. Indeed, the fluorescence signal intensity from the bacteria in diluted samples was larger (at the same intensity of light).

These observations confirm that the reactive oxygen created by the presence of fluorophore compromises the motility of bacteria. As expected when we applied the same experimental condition used in [12] (0.01 mM SYTO 9 and OD 0.4), the speed of the bacteria in solution with oxygen slows down to around $4\,\mu$m/s before stopping. Furthermore, the motility of bacteria is not affected by light when all oxygen is exhausted in the chamber. This phenomenon explains why the speed of the bacteria in the isotropic phase (in presence of oxygen) differs in the two experiments and also, why the speed of the bacteria in the anisotropic phase (in absence of oxygen) is similar in both publications.

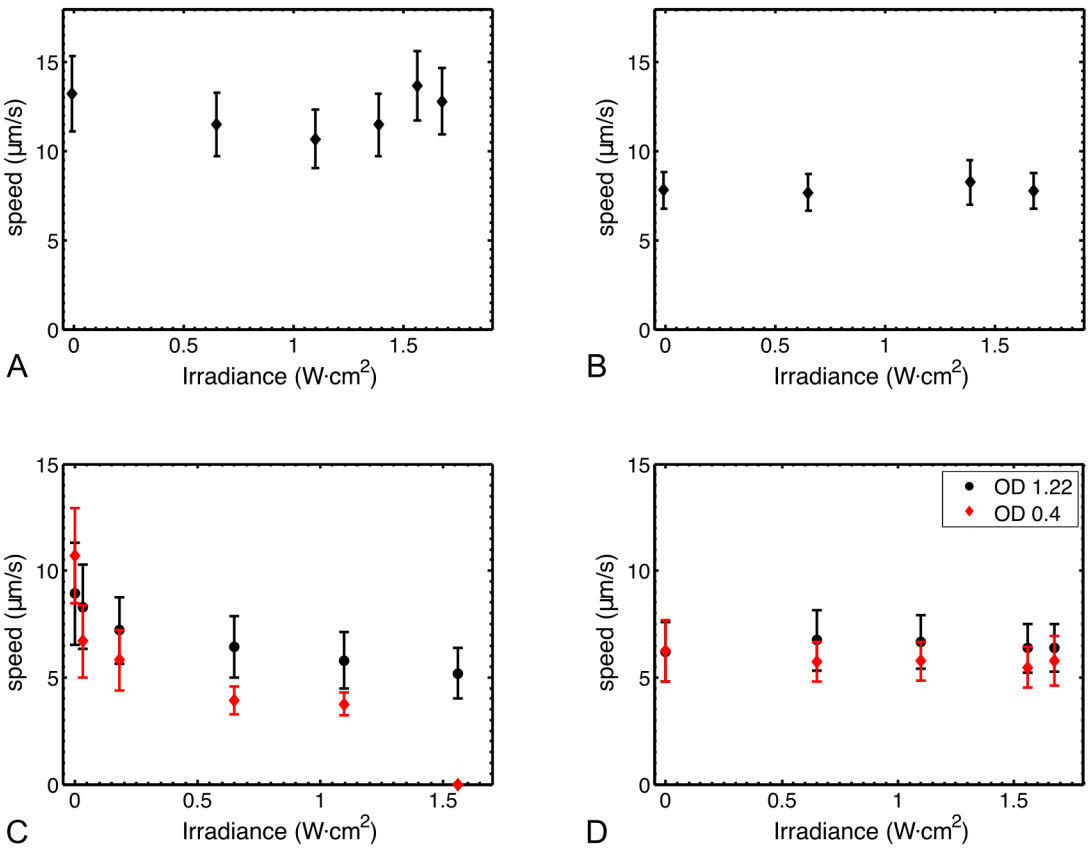

Figure S4: Effect of the reactive oxygen on the speed of the bacteria. Bacterial speed as a function of light intensity in motility buffer (A) with and (B) without the presence of oxygen. Bacterial speed as a function of the intensity of the light in motility buffer with 0.01 mM of Syto 9 (C) with and (D) without the presence of oxygen. Two sets of measurements are presented in C and D, one at high bacterial concentration (red diamonds) and the other at lower bacterial concentration. All experiments were performed at $22.5 \pm 0.5\,^{\circ}\mathrm{C}$.

S5 Typical Images

S5.1 Pretransition zone

This section shows bright field images of bacteria swimming in DSCG solutions (in motility buffer) in the pretransition zone. In each sequence, the images taken between parallel polarizers are all shown with the same intensity scale (the intensity scale is at the bottom right of the first image of each sequence). It is important to note that the images taken between crossed polarizers are shown with a different intensity scale to highlight how uniform these images are. The angle between the first polarizer and the x axis is reported on top of each image. The birefringence of our objective was corrected (in images taken between crossed polarizers) by using a sample at 0 wt % as calibration. All experiments were made at $22.5 \pm 0.5\,^{\circ}$C.

To quantify the isotropy of the LC samples in the pretransition zone (and rule out the presence of nematic domains), the extinction ratio was compared between images from the pretransition zone and the nematic phase. To do so, the intensity of each pixel of an image taken between parallel polarizers was divided by the intensity of images taken between perpendicular polarizers. The average and minimum extinction ratio r_e are reported in Table S2. The values in the pretransition zone are similar to those of the solution at 0 wt%. However, the minimum extinction ratio obtained in an inhomogeneous solution (at 10.2 wt%, see Fig. S8) is much smaller than those computed in the pretransition zone. Since this smaller minimum extinction ratio is caused by the presence of non-aligned nematic domains (see Fig. S8), this difference demonstrates that no small nematic domains are present in the pretransition zone. Furthermore, by observing the images taken between crossed polarizers in Figs. S5 and S7, no nematic domain can be seen (no bright zone similar to Fig. 3 *D* and *F* of the paper can be found in any image). We conclude that our solutions were always isotropic and homogeneous in the pretransition zone.

Table S2: Extinction ratio r_e of DSCG samples with bacteria. Extinction ratio, from 0 wt% to 9.2 wt% of DSCG, calculated with polarizer axis at 0° and 45° were similar, so we averaged their values.

Concentration (±0.2) (wt %)	Angle of the polarizer	r_e mean	r_e min
0	0° and 45°	15.5	11.0
7.2	0° and 45°	13.8	8.7
8.2	0° and 45°	16.0	9.8
9.2	0° and 45°	15.0	8.3
10.2	0°	11.2	1.7
10.2	45°	6.4	1.2
13.2	0°	12.2	2.3
13.2	45°	2.0	0.44

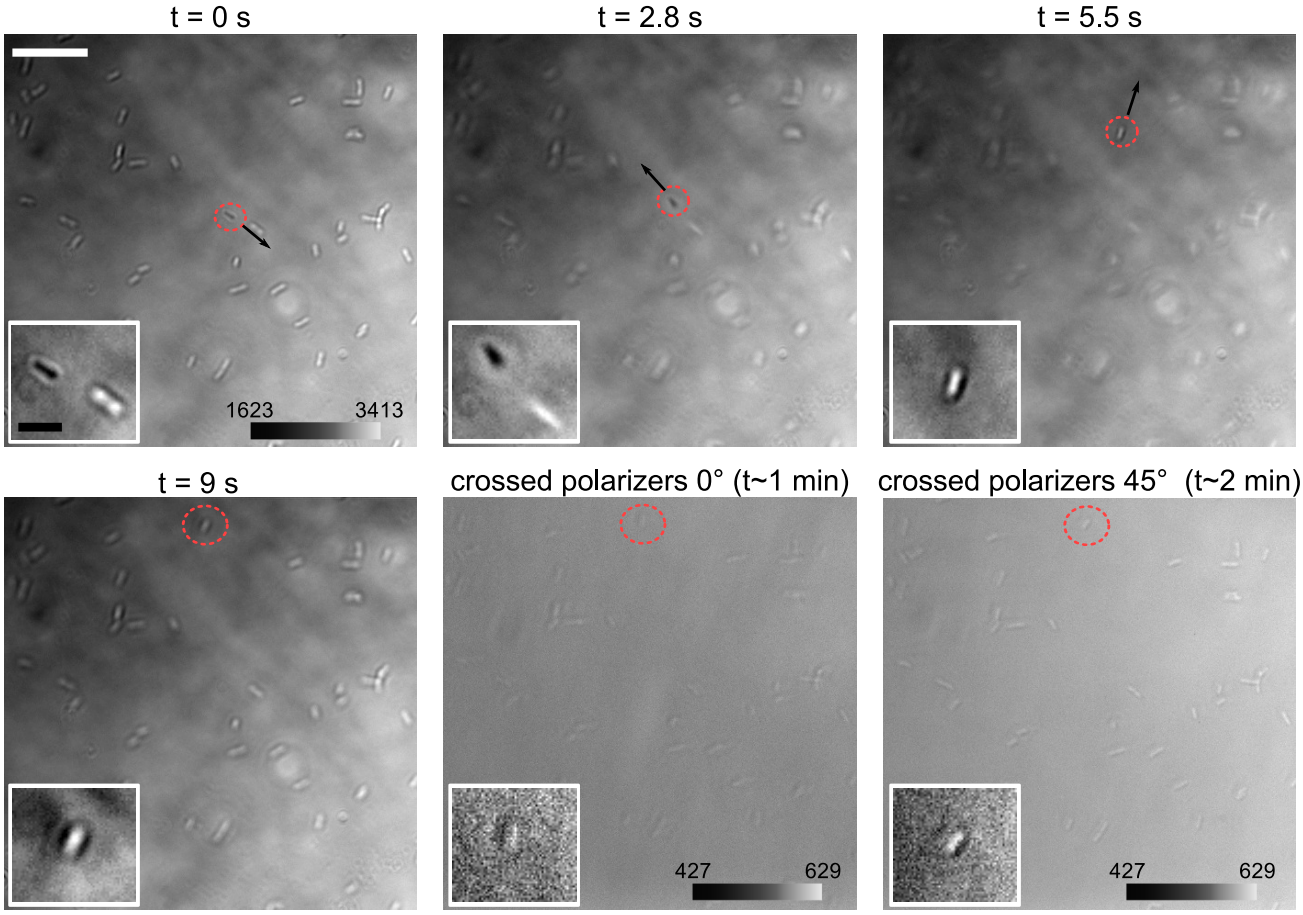

Figure S5: Sequence of images taken from a sample of bacteria with 7.2 wt% of DSCG. The sequence shows a swimming bacterium (circled in red) that remains stuck to the wall of the chamber at $t = 9\,\mathrm{s}$. The zoom of the region close to the swimming bacterium is shown (with enhanced contrast) in the white box at the bottom left of each image. Note that the movement of the bacterium in the z axis can be observed by the color of its body (black is further from the surface and white nearer). The first four images were taken between parallel polarizers (oriented at 0° from the x axis). The white scale bar (top left of the first image) measures $20\,\mu\mathrm{m}$ and the black bar (inset in the first image) measures $5\,\mu\mathrm{m}$.

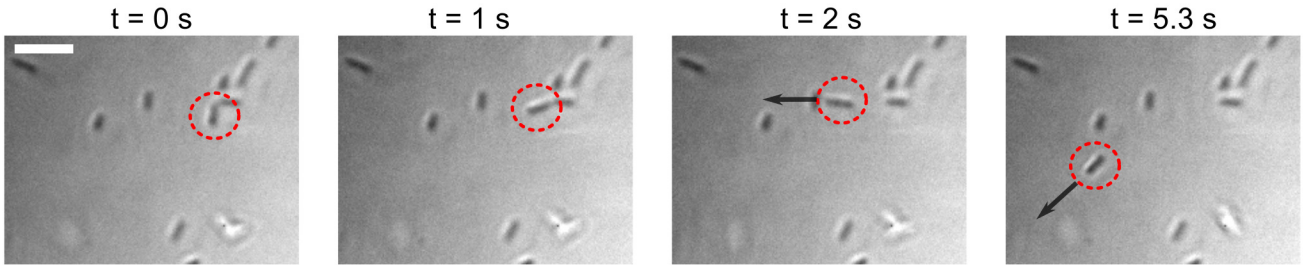

Figure S6: Sequence of images taken from a sample of bacteria with 7.2 wt% of DSCG showing the escape of a bacterium (circled in red) from an aggregate. All images were taken between parallel polarizers (oriented at 0° from the x axis). The white scale bar (top left of the first image) measures $10\,\mu\mathrm{m}$.

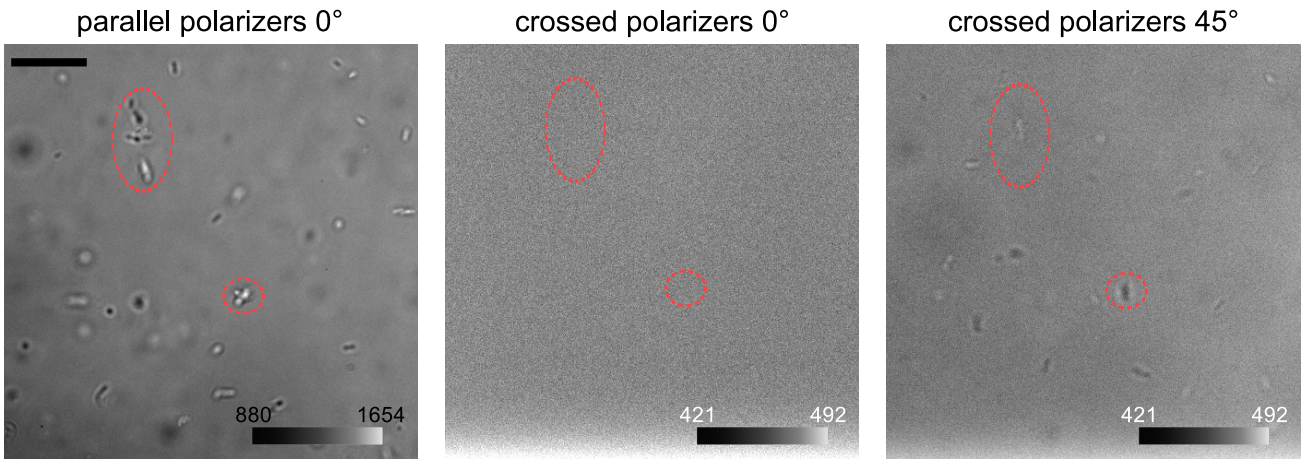

Figure S7: Sequence of images taken from a sample of bacteria with 8.2 wt% of DSCG showing two aggregates of bacteria (circled in red) in the medium (far from surfaces). The black scale bar (top left of the first image) measures 20 μm. Note the different intensity scale between the first image and the other two. This shows that the aggregates of bacteria are not caused by local inhomogeneities in the medium.

S5.2 Nematic phase

This section shows bright field images of microspheres in DSCG solutions (in MB) in the nematic phase and in the transition zone. The angle between the first polarizer and the axis of the director (the x axis in Fig. S8) is reported on top of each image, and the intensity scale is at the bottom right. From the images to the right of Fig. S9 we can conclude that DSCG aggregates in samples were well aligned (the intensity is high and uniform). All experiments were made at $22.5 \pm 0.5\,^{\circ}$C.

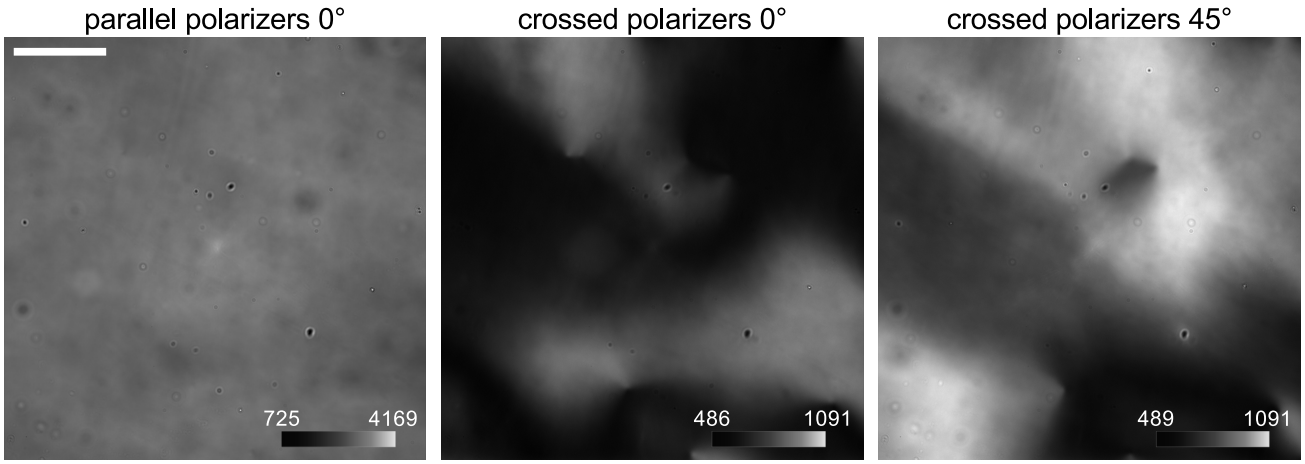

Figure S8: Images taken from a sample of microspheres with a diameter of $0.75\,\mu$m in a solution with 10.2 wt% of DSCG. The image presents a nematic section of the sample that was not well aligned, this is why the intensity is not uniform. The white scale bar (top left in the first image) measures $50\,\mu$m.

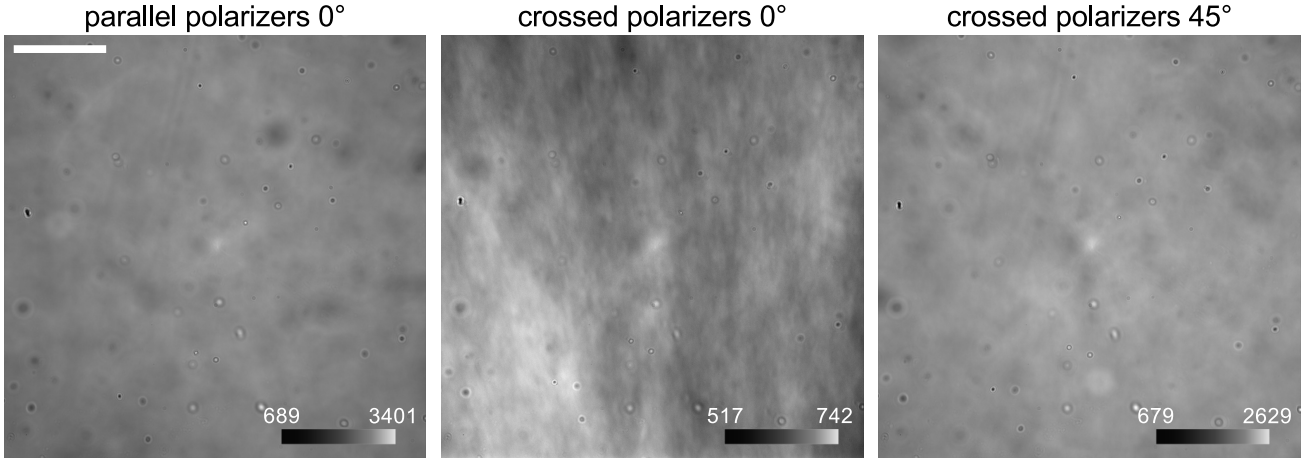

Figure S9: Images taken from a sample of microspheres with a diameter of $0.75\,\mu$m in a solution with 13.2 wt% of DSCG. The white scale bar (top left in the first image) measures $50\,\mu$m.

S6 Additional figures and tables

Table S3: Number of tracked bacteria and total number of recorded positions for each DSCG concentration.

Concentration (±0.2) (wt %)	Number of tracked bacteria	Total number of recorded positions
0	426	12265
1	221	6823
2.1	189	4973
3.2	134	3583
4.2	166	5981
5.3	180	6964
6.3	101	4112
7.4	85	3157
8.4	41	2519
9.5	37	2843
10.5	111	11616
11.6	40	6805
12.6	34	4393
13.7	43	7916

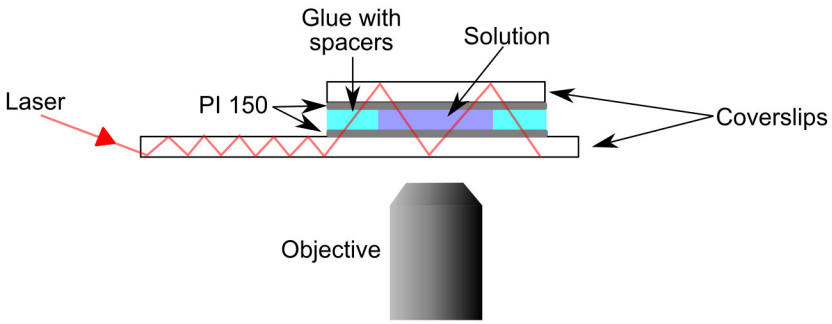

Figure S10: Scheme of a cell used for the observation of bacteria and for the measurement of DSCG solution's viscosity. The principle of light guided dark-field microscopy is illustrated with the laser beam (see also [3]).

Table S4: Constants used for the calculation of the DSCG aggregates length.

Constant name	Symbol	Value or equation
Viscosity at 0 wt%	η_0	$0.96\,\mathrm{g/m \cdot s}$
Viscosity of the solution	η	—
Relative viscosity	η_r	$\frac{\eta}{\eta_0}$
Radius of DSCG disk	r	1 nm
Thickness of DSCG disk	d	0.34 nm
Stokes radius of DSCG disk	r_p	0.55 nm
Volume fraction of molecule in aggregates	ϕ_m	0.9
Volume fraction of DSCG	ϕ	—
Fractal dimension of aggregates	d_f	1
Hydrodynamic volume of aggregates	v_h	$\frac{M}{N_a}$

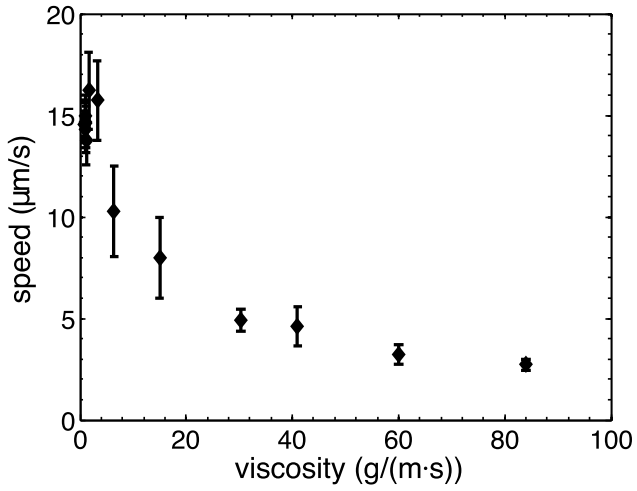

Figure S11: Speed of the bacteria as a function of the viscosity parallel to the director.

SUPPORTING REFERENCES

[1] Turiv, T., I. Lazo, A. Brodin, B. I. Lev, V. Reiffenrath, V. G. Nazarenko, and O. D. Lavrentovich. 2013. Effect of collective molecular reorientations on brownian motion of colloids in nematic liquid crystal. *Science*. 342:1351–1354.

[2] Berezhkovskii, A. M., L. Dagdug, and S. M. Bezrukov. 2014. Discriminating between anomalous diffusion and transient behavior in microheterogeneous environments. *Biophys. J.* 106:L09–L11.

[3] Duchesne, I., S. Rainville, and T. Galstian. 2015. Application of a microrheology technique to measure the viscosity of disodium cromoglycate liquid crystal. *Mol. Cryst. Liq. Cryst.* Submitted.

[4] Sowa, Y. and R. M. Berry. 2008. Bacterial Flagellar Motor. *Q. Rev. Biophys.* 41:103–132.

[5] Martinez, V. A., J. Schwarz-Linek, M. Reufer, L. G. Wilson, A. N. Morozov, and W. C. K. Poon. 2014. Flagellated bacterial motility in polymer solutions. *Proc. Natl. Acad. Sci. USA*. 111:17771–17776.

[6] Purcell E. M. 1997. The efficiency of propulsion by a rotating flagellum. *Proc. Natl. Acad. Sci. USA*. 94:11307–11311.

[7] Chattopadhyay, S., R. Moldovan, C. Yeung, and X. L. Wu. 2006. Swimming efficiency of bacterium *Escherichiacoli*. *Proc. Natl. Acad. Sci. USA*. 103:13712–13717.

[8] Mao, Y., M. E. Cates, and H. N. W. Lekkerkerker. 1997. Theory of the depletion force due to rodlike polymers. *J. Chem. Phys.* 106:3721–3729.

[9] Yaman K., C. Jeppesen, and C. M. Marques. 1998. Depletion forces between two spheres in a rod solution. *Europhys. Lett.* 42:221

[10] Hadjur, C., N. Lange, J. Rebstein, P. Monnier, H. van den Bergh, and G. Wagnières. 1998. Spectroscopic studies of photobleaching and photoproduct formation of *meta*(tetrahydroxyphenyl)chlorin (*m*-THPC) used in photodynamic therapy. The production of singlet oxygen by *m*-THPC. *J. Photochem. Photobiol. B, Biol.* 45:170–178

[11] Heiser, I., W. Oßwald, and E. F. Elstner. 1998. The formation of reactive oxygen species by fungal and bacterial phytotoxins. *Plant Physiol. Biochem.* 36:703–713

[12] Kumar, A., T. Galstian, S. K. Pattanayek, and S. Rainville. 2013. The motility of bacteria in an anisotropic liquid environment. *Mol. Cryst. Liq. Cryst.* 574:33–39.